Noncircular CFRP bicycle's chainring, part II: finite element analysis

Zhorachaid Thanawarothon, Abdelrahman Elmikaty, Christophe Bouvet, Laurent Mezeix

NONCIRCULAR CFRP BICYCLE'S CHAINRING. PART II: FINITE ELEMENT ANALYSIS

Zhorachaid Thanawarothon,[1] Abdelrahman Elmikaty,[2] Christophe Bouvet,[2] & Laurent Mezeix[1,]*

[1]*Faculty of Engineering, Burapha University, 169 Long-Hard Bangsaen Road, Chonburi 20131, Thailand*

[2]*Université de Toulouse, INSA, UPS, Mines d'Albi, ISAE, ICA (Institut Clément Ader), 135 Avenue de Rangueil, 31077 Toulouse Cedex, France*

*Address all correspondence to: Laurent Mezeix, Faculty of Engineering, Burapha University, 169 Long-Hard Bangsaen Road, Chonburi 20131, Thailand, E-mail: Laurent.mezeix@hotmail.com

In this paper, numerical simulation is developed in order to analyze the failure of a noncircular composite chainring, and teeth damage is especially detailed. Simulation consists of the chainring and a part of the metallic chain. To reduce the size of the numerical model only the first 11 rollers are simulated. In order to validate the numerical simulation, the force–displacement curve is compared with the experimental results obtained on the same specimens used in the simulation. Then, the effect of the noncircular shape is studied through three different loading positions, and a damage scenario is proposed. Moreover, the effect of composite lay-up is investigated through different lay-ups. The results show that the loading position has no influence on the chainring behavior, while the damage scenario depends on it. The damage consists of matrix cracking located on the teeth surface. Finally, the thickness can be reduced to 9 plies lay-up and even if the damage is larger, it is always located on the teeth surface.

KEY WORDS: *noncircular chainring, CFRP, FEA, matrix cracking*

1. INTRODUCTION

The use of Carbon Fiber Reinforced Polymers (CFRP) has significantly increased over the past 40 years in aerospace, structural engineering, land transports, and sport industries. Indeed, thanks to their mechanical properties, i.e., high modulus and strength and low density, gain of mass is expected. Although CFRP present better properties than aluminum, impact (Bouvet and Rivallant, 2016; Rozylo et al., 2017) and edge damage (Ostré et al., 2016; Li and Chen, 2016) are major concerns due to the influence on the residual mechanical properties of the structure.

Sport industry uses more and more composite materials in order to increase the specific strength of the equipment. CFRP tennis rackets and baseball bats are replaced by wood (Brody, 1997). Carbon/epoxy golf clubs are used to reduce the weight and to increase the ball exit velocity (Slater et al., 2010). Snowboarding, surfing and other boardsports take advantage of a composite material to increase the stiffness/weight ratio (Clifton et al., 2010). Performance of professional bike increased by using CFRP instead of aluminum to obtain a high stiffness and strength frame at low weights (Jin-Chee and Wu, 2010). In the last decade, bike wheels started also to be proposed in CFRP to reduce the weight and to provide smoother ride (Peter, 2013). Noncircular chainrings allow one to increase the power output while cycling and therefore they had shown interest (Bini and Dagoese, 2012; Rankin and Neptune, 2008). Indeed, B. Wiggins and C. Froome won Tour de France with an oval rings in 2011 and with an osymetric chainring since 2013, respectively[**Q1**]. Chainring is commonly manufactured of aluminum alloy but recently a noncircular carbon composite chainring made of 11 carbon woven/epoxy plies was experimentally studied (Thanawarothon et al., 2018). The results showed that under quasi-static tension, the metallic chain firstly failed. Low-velocity/low-energy impact on the teeth was also investigated and for an energy higher than 1.6 J delaminations were observed by C-Scan.

Due to the complex shape of the teeth, a composite damage cannot be detected easily experimentally by a Non Destructive Test. Therefore, numerical simulation has been developed in this paper to determine the teeth failure mechanism of noncircular composite chainring under quasi-static loads. The aim is to use this model as a design tool to optimize noncircular composite chainring. In order to validate the FEA construction, the simulation is compared with experimental results obtained previously by the same authors. Then, noncircularity effect is investigated through three loading cases. Finally, thanks to the simulation, the stacking influence is proposed to find the best lay-up.

2. MODEL CONSTRUCTION AND VALIDATION

2.1 Chainring and Chain

Noncircular composite chainring with 53 teeth are studied in this paper (Fig. 1). The radius of the noncircular chainring depended on the angle θ (Table 1). The teeth design proposed by Wang is used for the chainring (Wang et al., 2013). The chain consisted of rollers, inner and outer plates (Fig. 2), and it is provided by SRAM (reference PC-991). The failure of the chain is given for a force of 9000 N by the manufacturer (SRAM, 2018). The roller diameter is 7.77 mm (0.306 in) and the chain pitch is 12.7 mm (0.5 in).

The aim of the simulation is to determine the failure scenario of the noncircular composite chainring. The FE model consisted of the chainring, and a part of the chain was modelled with C3D8R solid elements. The literature showed that the loading is

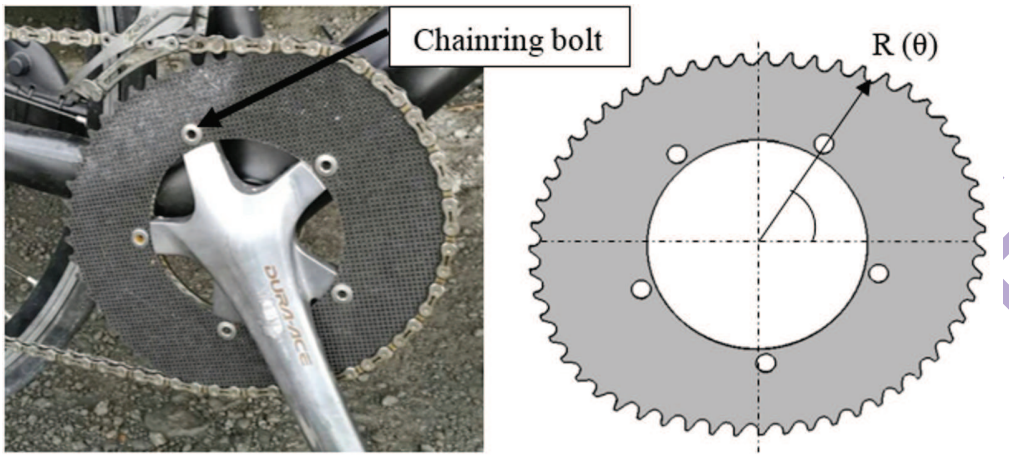

FIG. 1: Composite and model of noncircular chainring

TABLE 1: Radius of the noncircular chainring

Angle, θ [°]	*R* [mm]	Angle, θ [°]	*R* [mm]	Angle, θ [°]	*R* [mm]
0	93.97	70	105.58	140	97.05
10	95.23	80	106.38	150	94.11
20	96.77	90	106.73	160	92.99
30	98.59	100	106.90	170	93.13
40	100.54	110	106.94	180	93.97
50	102.50	120	105.79	—	—
60	104.25	130	101.24	—	—

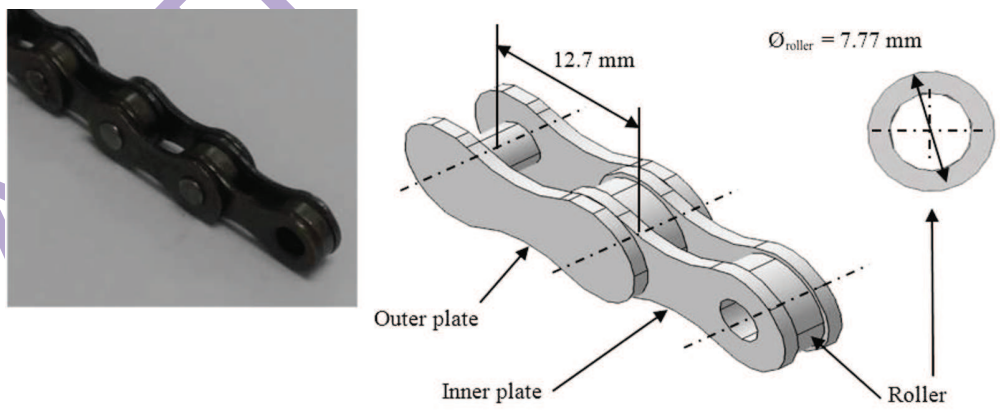

FIG. 2: Chain and chain model

mainly concentrated on the first seven teeth (Huo et al. 2013). Thus, in this paper, the first eleven rollers were simulated in order to reduce the computing time (Fig. 3). Moreover, the mesh around these eleven rollers was refined to obtain more accurate results (Fig. 4). To simulate the chainring bolt (Fig. 1), encastré[**Q2**] boundary con-

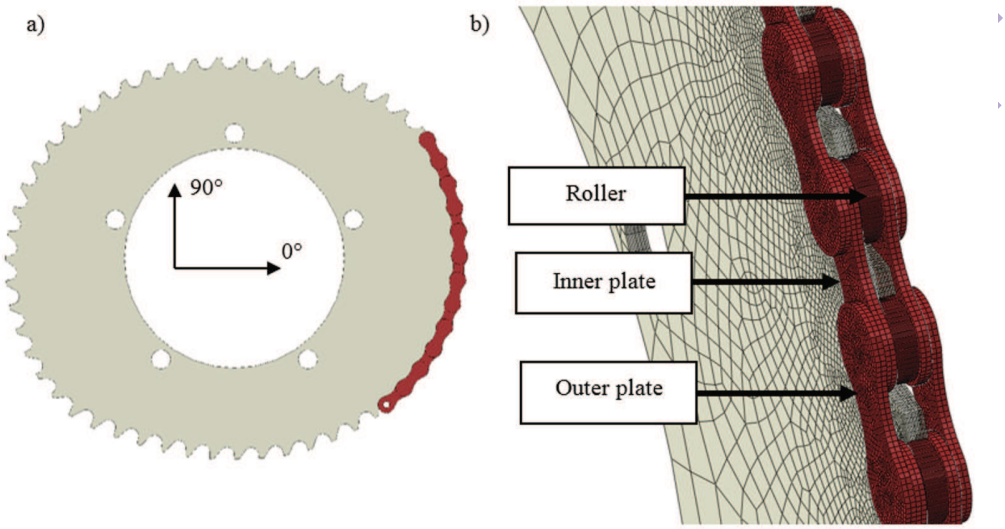

FIG. 3: General view (a) and details (b) of the chain and chainring of simulation

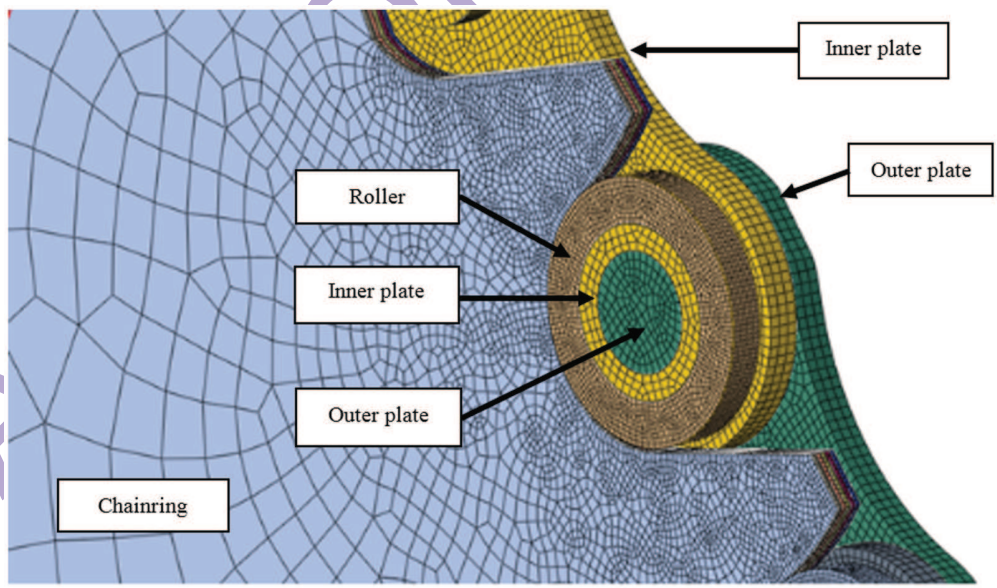

FIG. 4: View cut of the chain and chainring with mesh details

dition is applied (Fig. 5). Normal behavior is used as contact property in ABAQUS between the chain and the chainring. The scope of this work is the quasi-static me-

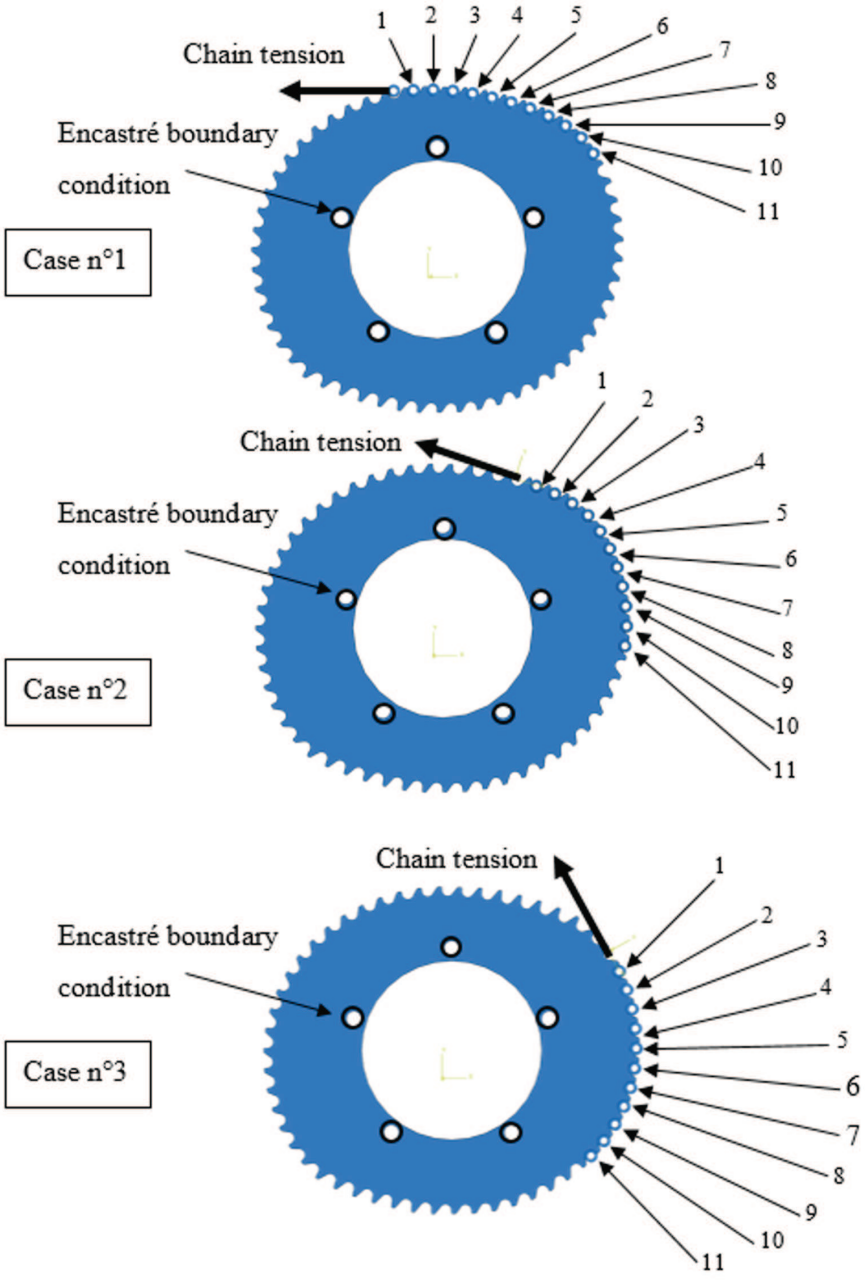

FIG. 5: Loading positions for noncircular chainring

chanical strength of noncircular chainring, and so the friction between the teeth and the chairing is not considered. Due to the shape of the noncircular chainring, three chain positions are investigated (Fig. 5). The chain is assumed to be stretched, and the tangential loading representing its tension force is applied.

2.2 Materials Properties

The chain is made of steel (Table 2), while carbon 2/2 twill woven/epoxy is used for the chainring (Table 3). The chainring consists of 11 plies of 0.23 mm each with the following stacking: [30/60/0/60/30/0/30/60/0/60/30], given a chainring thickness of 2.53 mm after manufacturing (Fig. 6).

As delamination was not observed in previous experiments, only fiber failure and matrix cracking are modelled thanks to the nonlinear modeling. Failure criteria associated to failure modes are used (Camanho, 2002). Thus, fiber failure is calculated thanks to the maximum stress criteria for the longitudinal and transverse direction, and it is given by

$$\frac{\sigma_l}{\sigma_l^{f,t}} = 1, \tag{1}$$

TABLE 2: Steel properties (Azo Materials, 2013)

Material	E [GPa]	η	σ_y [MPA]	ρ [kg/m^3]
HSS Steel	220	0.30	500	8000

TABLE 3: Carbon 2/2 twill woven/epoxy ply properties

Carbon/Epoxy (T300/EPOTEC YD 535 LV, TH 7253-8)	
Tensile Young's modulus in fiber direction	35 GPa
Compressive Young's modulus in fiber direction	–35 GPa
Transverse Young's modulus	35 GPa
Shear modulus	4.3 GPa
Poisson's ratio	0.05
ρ [kg/m^3]	1700
Failure	
Longitudinal tensile strength	750 MPa
Longitudinal compressive strength	–750 MPa
Transverse tensile strength	750 MPa
Transverse compressive strength	–750 MPa
In-plane shear strength	98 MPa
Out-of-plane shear strength	50 MPa

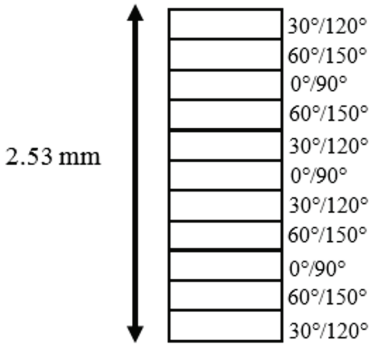

FIG. 6: Eleven plies stacking of noncircular composite chainring

$$\frac{\sigma_t}{\sigma_t^{f,t}} = 1. \tag{2}$$

The matrix cracking criterion is computed thanks to

$$\frac{\tau_{lt}^2 \tau_{tz}^2}{\tau_{lt}^{f\,2}} = 1, \tag{3}$$

where σ_l, σ_t, τ_{lt}, and τ_{tz} are respectively the longitudinal and transverse stress, the shear stress in the (l, t) plane, and the shear stress in the (t, z) plane, evaluated in the neighboring volume elements, $\sigma_t^{f,t}$ is the transverse failure stress in tension, and τ_{lt}^f is the failure shear stress. These criteria are assessed at each time increment, and, when the longitudinal or transverse stress reaches the associated strength, the following stiffness matrix parameter become zero: Q_{11}, Q_{12}, and Q_{13} for the longitudinal direction and Q_{22}, Q_{12}, and Q_{23} for the transverse direction. For matrix cracking Q_{55} and Q_{66} become zero. Failure modes can be predicted by these criteria, and therefore a progressive damage analysis can be adequately used. Thus, the FE model employs explicit integration scheme in ABAQUS. Experimental results on the same noncircular chainring showed a linear behavior until a force of 4500 N where the chain starts damaging (Thanawarothon et al., 2018). In the present paper, an analysis is realized until the chain damage, and therefore, the chain behavior is modeled using the isotropic elastic laws behaviors. Composite chainring properties are programmed using FORTRAN and input to ABAQUS in the form of a 'user material' (VUMAT) subroutine.

2.3 Model Validation

In order to validate the simulation, the force–displacement curve obtained from the simulation is compared to the experimental results obtained on the same noncircular composite chainring for case 3 only (Thanawarothon et al., 2018).The similarity of the curves shows that the model is able to be reproduced until the chain damage, the global response of tensile test of a noncircular composite chainring (Fig. 7). Two dis-

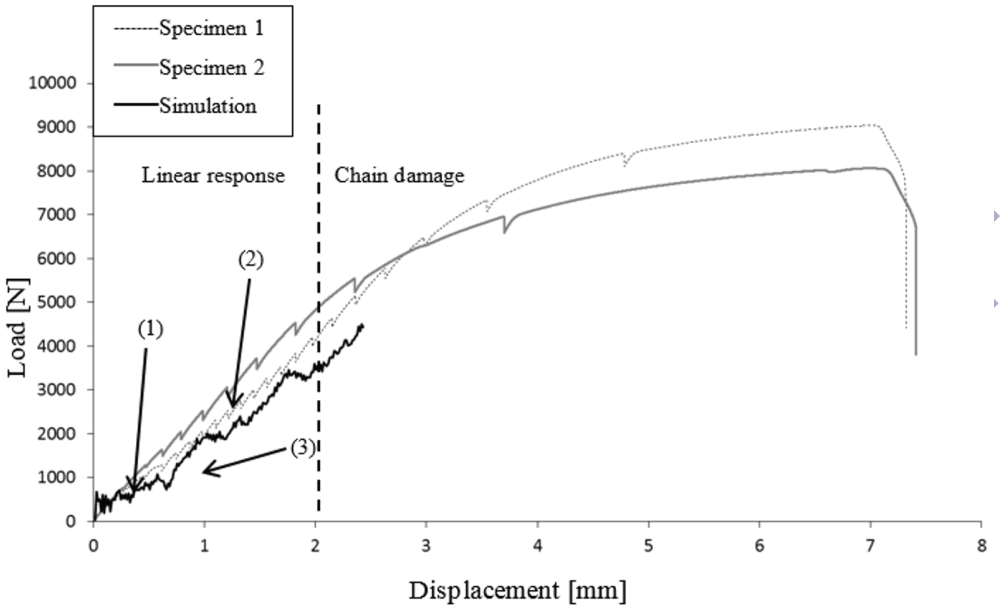

FIG. 7: Comparison of force–displacement graphs for case 3

tinct phases can be identified from the simulation curves. In the beginning, an elastic response is exhibited (1) until a force of 500 N where the force drops. Then the force increases linearly until the chain damage (2). Drop of force is observed for a force of 1150 N (3).

3. RESULTS AND DISCUSSIONS

3.1 Noncircularity Effect

As the chainring is not circular, effect of the loading position is studied (Fig. 5). However, loading position does not show the influence on the chainring behavior (Fig. 8). The curves indicate a first linear domain (1) corresponding to the contact between the first roller and the first tooth. Then, the force oscillates due to the successive contact between the first five rollers and the associated teeth (2). Drop of force observed experimentally (Fig. 6) is due to the contact of rollers from the 8th to 11th with the chainring (3).

Due to the pressure of the rollers on the teeth, teeth failure consists only of matrix cracking given by Eq. (3). Therefore, first failure appears in the tooth where the shear stress is the maximum. For case 1, failure initiates on the 6th tooth and then propagates to the first tooth. The first failure for case 2 appears in the 2nd tooth, then the 1st one fails followed by the 4th one. For both cases, failure seems to start in

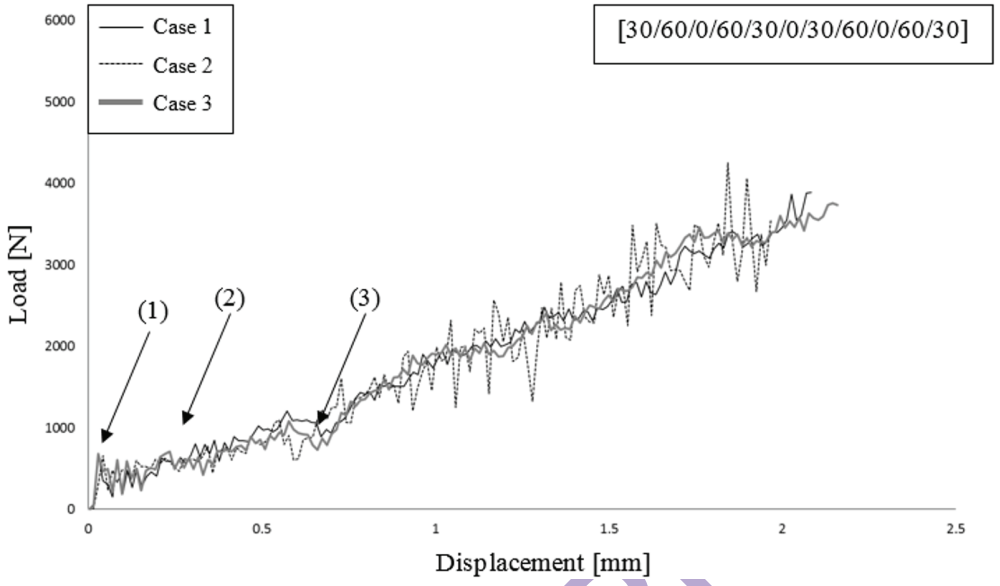

FIG. 8: Force–displacement curves for different loading cases obtained by the simulation

the same area. Indeed, the 6th and 2nd tooth of cases 1 and 2, respectively, are both located at the beginning of the curve part of the noncircular chainring (Fig. 5). Case 1 presents a different behavior where the 4th tooth firstly fails. Then, the failure progress from the 1st to the 6th. Cases 1 and 3 show a first failure for a similar load, while for case 2 the failure appears for a lower value (Table 4). However, loading position does not have influence on the next teeth load failure. Matrix cracking is located only on the surface of the teeth where contacts are made with rollers (Fig. 9). Finally, FEA shows that until the chain starts damaging, i.e., for a load of 4500 N (Thanawarothon et al., 2018), teeth present only local matrix cracks.

TABLE 4: Failure scenario and associated force

Failure Scenario	Case 1	Case 2	Case 3
First tooth failure	6 (2300 N)	2 (1450 N)	4 (2200 N)
Second tooth failure	3 (2500 N)	1 (2600 N)	1 (2300 N)
Third tooth failure	1 (2800 N)	4 (2800 N)	2 (2600 N)
Fourth tooth failure	2 (3300 N)	—	6 (3500 N)

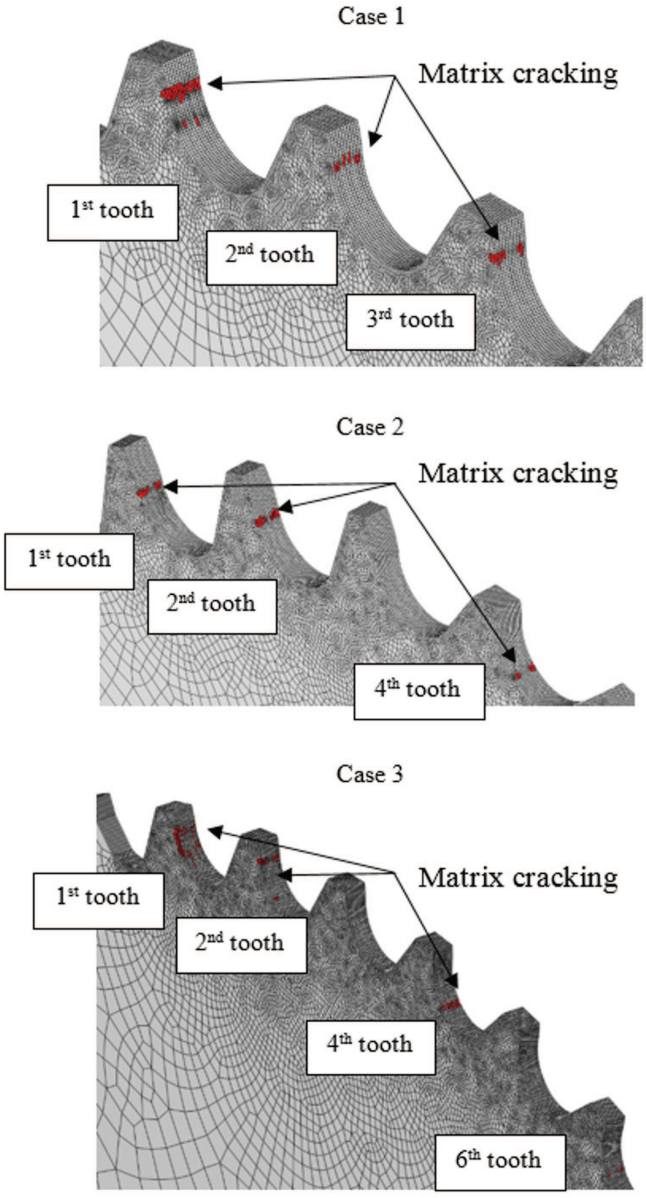

FIG. 9: Matrix cracking given by Eq. (3) for three loading positions and for a force of 3700 N

Damage propagation in teeth can be studied. Evolution is the same for all teeth and the 2nd tooth of case 2 is proposed as an example in Fig. 10. Matrix cracking always starts in the 2nd and 10th plies (60°/150°) and then, the damage propagates mainly to the adjacent interior plies.

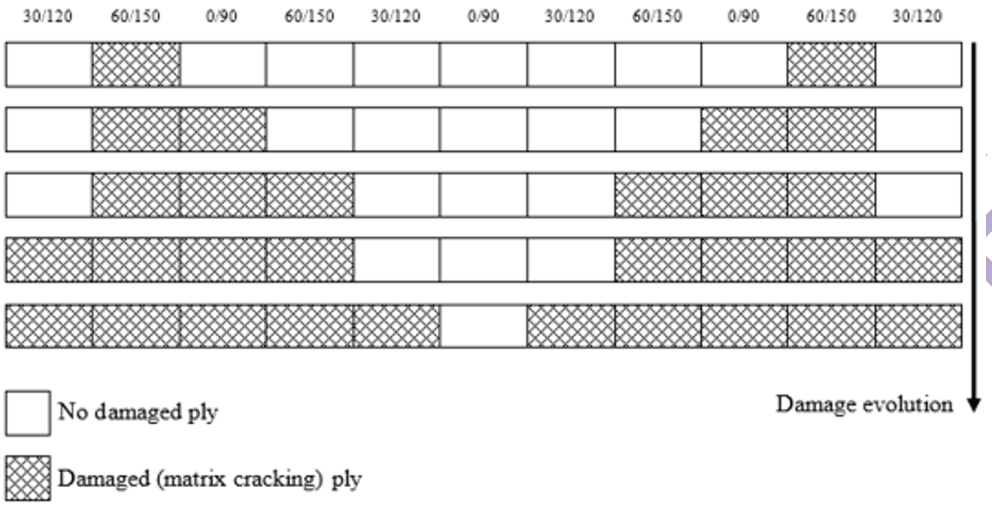

FIG. 10: Evolution of the matrix cracking in the 2nd tooth of case 2

3.2 Stacking Effect

Effect of the lay-up is investigated through a second 11 plies stacking: $[45_2/0/45_2/0/45_2/0/45_2]$. Similar behavior as the previous stacking is observed (Fig. 11), and moreover, loading position does not show influence. Indeed, as the

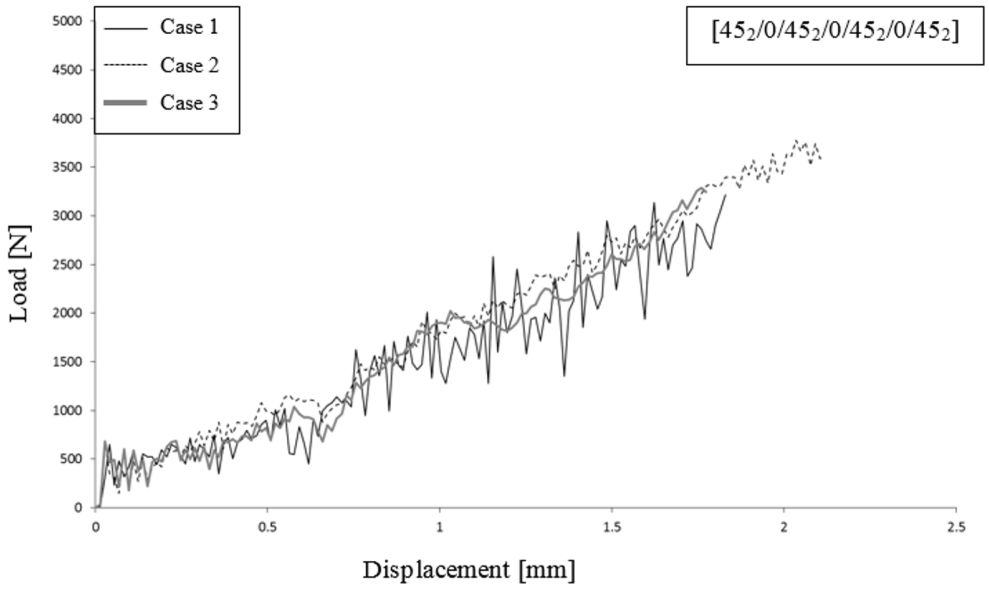

FIG. 11: Force–displacement curves for different loading cases obtained by the simulation

matrix cracking is observed only on the surface of the teeth, it is too small to have an effect. However, damage seems to be lightly reduced compared to the first lay-up (Fig. 12). For loading case 3, no matrix cracks are observed in the 6th tooth (Table 5).

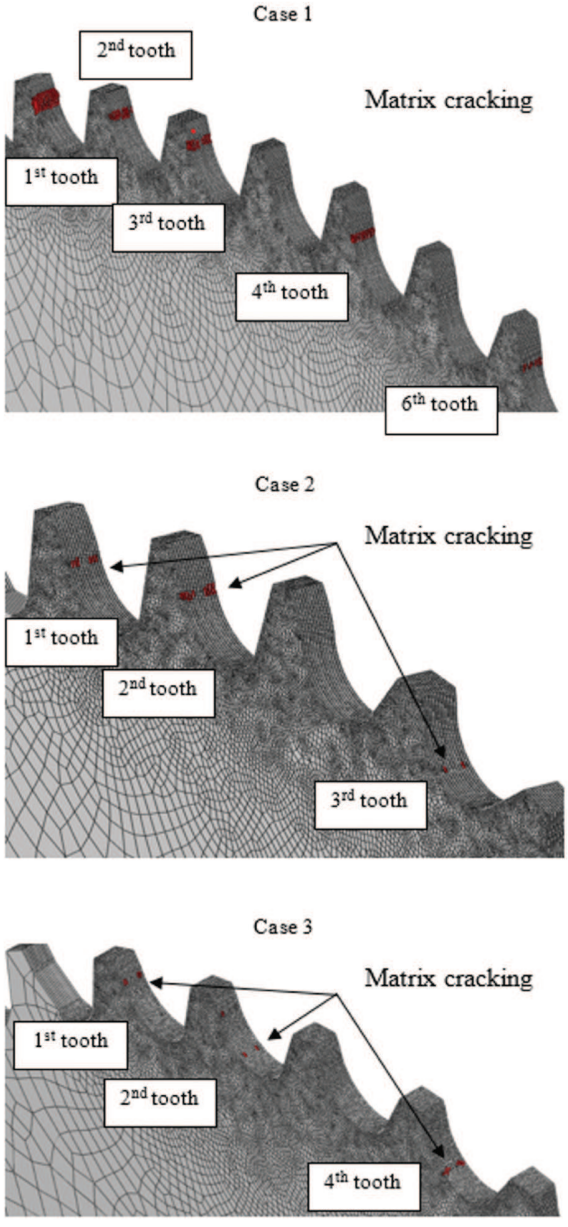

FIG. 12: Matrix cracking given by Eq. (3) for three loading positions for $[45_2/0/45_2/0/45_2/0/45_2]$ lay-up and for a force of 3500 N

TABLE 5: Failure scenario and associated force for $[45_2/0/45_2/0/45_2/0/45_2]$ lay-up

Failure Scenario	Case 1	Case 2	Case 3
First tooth failure	6 (2300 N)	2 (1300 N)	4 (2200 N)
Second tooth failure	3 (2500 N)	1 (200 N)	1 (2500 N)
Third tooth failure	1 (2800 N)	4 (2800 N)	2 (3000 N)
Fourth tooth failure	2 (3400 N)	—	—

Evolution of the matrix cracking is similar to those observe for the previous 11 plies lay-up (Fig. 10).

3.3 Thickness Effect

Eleven plies composite chainring showed only matrix cracking located on the teeth surface. Therefore, the number of plies can be reduced in order to minimize the chainring cost. Due to the chain size, reduction of plies number is limited. Thus, effect of the number of plies is studied through a 9 plies stacking: $[45_2/0/45_3/0/45_2]$. Moreover, as the loading case does not show influence, only loading case 3 is investigated (Fig. 13). A similar behavior as the previous stacking is observed. However, matrix cracking is

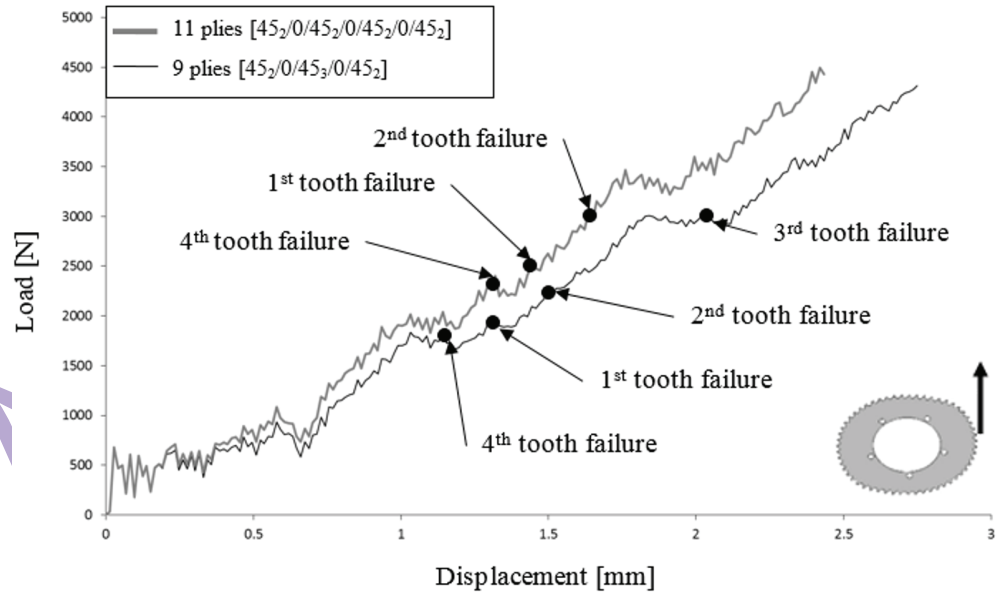

FIG. 13: Force–displacement curves for loading case 3 with 9 and 11 plies stacking obtained by simulation

observed for a lower force, and due to the lower number of plies the teeth damage is bigger (Fig. 14). Indeed, for the 9 plies stacking the fourth firsts teeth are damaged while for the 11 plies stacking only the three firsts show matrix cracking.

Damage propagation in teeth can be studied for the 9 plies lay-up. As for the 11 plies, evolution is the same for all teeth and the 4th tooth of case 3 is proposed as example (Fig. 15). Matrix cracking starts always in the 3rd and 7th plies (0°/90°) and then, the damage propagates symmetrically to these plies.

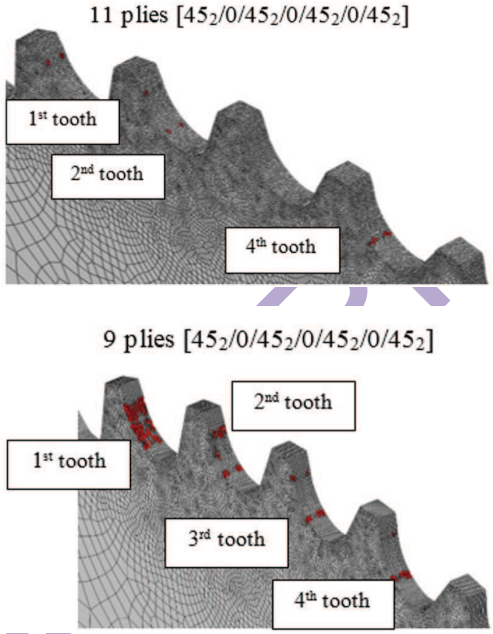

FIG. 14: Matrix cracking given by Eq. (3) for loading case 3 with a stacking of 11 and 9 plies

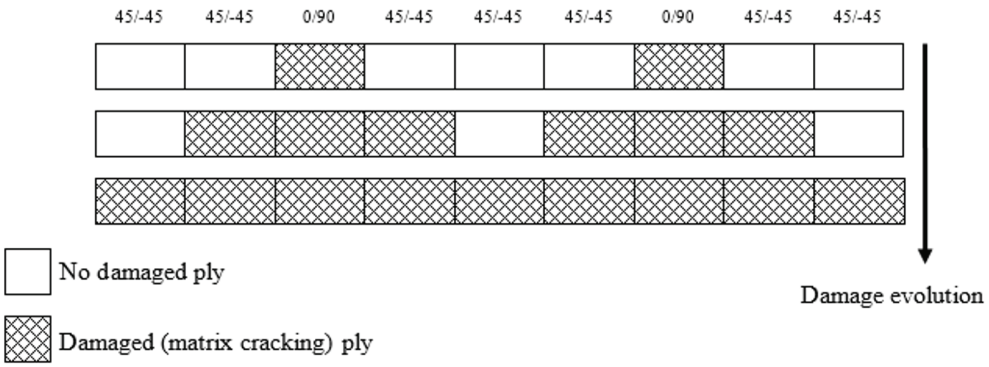

FIG. 15: Evolution of the matrix cracking in the 4th tooth of case 3 for 9 plies lay-up

4. CONCLUSIONS

In order to design and optimize noncircular composite chainring, a numerical simulation has been proposed to determine the failure scenario of teeth. The chainring and 11 rollers of the chain have been modeled using an explicit simulation. Three loading positions were performed in order to study the effect of the noncircular chainring shape. CFRP made of 11 plies of carbon woven/epoxy was investigated, and maximum stress has been used as failure criteria for the composite material. According to the numerical simulation, the mechanical behavior of the noncircular chainring can be concluded as follows:

- The noncircularity has no influence on the mechanical behavior.
- The damage scenario has been determined and it depends of the loading position. However, until the chain damage, i.e., 4500 N, teeth damage consists only of matrix cracking located on the teeth surface.
- As the damage is only located on teeth surface, the chainring behavior is not influenced by the lay-up until the chain damage.
- The thickness can be reduced to 9 plies. Even if the matric cracking is larger than on 11 plies chainring, the damage is always located on the teeth surface.

Under quasi-static condition, noncircular composite chainring made of 11 plies does not fail. Indeed, only local matrix cracking are observed on the contact surface with the roller. Therefore, thickness can be lightly reduced to 9 plies in order to minimize the chainring cost. However, experiments showed that 1.6 J low-velocity impact located on a tooth creates delamination that could reduce the final strength of the noncircular composite chainring. The low-velocity impact has to be investigated on 9 plies stacking to determine the damage. The proposed numerical model is currently under development to simulate a low-velocity impact, especially to obtain delaminations in order to determine their influence on the residual chainring strength.

REFERENCES

Azo Materials, From http://www.azom.com, 2012.

Bini, R.R. and Dagoese, F., Noncircular Chainrings and Pedal to Crank Interface in Cycling: A Literature Review, *Braz. J. Kinantropom. Hum. Perform.*, vol. **14**, pp. 470–482, 2012.

Bouvet, C. and Rivallant, S., Damage Tolerance of Composite Structures under Low-Velocity Impact, in: V. Silberschmidt, Ed., *Dynamic Deformation, Damage and Fracture in Composite Matererials and Structures,* Woodhead Publishing, pp. 7–33, 2016.

Brody, H., The Physics of Tennis. III: The Ball–Racket Interaction, *Am. J. Phys.*, vol. **65**, pp. 981–987, 1997.

Camanho, P.P., *Failure Criteria for Fiber-Reinforced Polymer Composites*, from https://web.fe.up.pt/~stpinho/teaching/feup/y0506/fcriteria.pdf, 2002.

Clifton, P., Subic, A., and Mouritz, A., Snowboard Stiffness Prediction Model for any Composite Sandwich Construction, *Proced. Eng.*, vol. **2**, pp. 3163–3169, 2010.

Huo, J., Yu, S., Yang, J., and Li, T., Static and Dynamic Characteristics of the Chain Drive System of a Heavy Duty Apron Feeder, *Open Mech. Eng. J.*, vol. **7**, pp. 121–128, 2013.

Jin-Chee Liu, T. and Wu, H.C., Fiber Direction and Stacking Sequence Design for Bicycle Frame made of Carbon/Epoxy Composite Laminate, *Mater. Des.*, vol. **31**, pp. 1971–1980, 2010.

Li, N. and Chen, P.H., Experimental Investigation on Edge Impact Damage and Compression-After-Impact (CAI) Behavior of Stiffened Composite Panels, *Compos. Struct.*, vol. **138**, pp. 134–150, 2016.

Ostré, B., Bouvet, C., Minot, C., and Aboissière, J., Finite Element Analysis of CFRP Laminates Subjected to Compression after Edge Impact, *Compos. Struct.*, vol. **153**, pp. 478–489, 2016.

Peter, *Carbon Fiber Bikes vs. Aluminum Bikes. Which Should You Buy?* From http://www.over40cyclist.com/carbon-fiber-bikes-vs-aluminum-bikes/, 2013.

Rozylo, P., Debski, H., and Kubiak, T., A Model of Low-Velocity Impact Damage of Composite Plates subjected to Compression-After-Impact (CAI) Testing, *Compos. Struct.*, vol. **181**, pp. 158–170, 2017.

Slater, C., Otto, S.R., and Strangwood, M., The Quasi-Static and Dynamic Testing of Damping in Golf Clubs Shafts Fabricated from Carbon Fiber Composites, *Proced. Eng.*, vol. **2**, pp. 3361–3366, 2010.

SRAM, PC-991 Chain, https://www.sram.com, 2018.

Thanawarothon, Z., Pairat, P., Bouvet, C., and Mezeix, L., Noncircular CFRP Bicycle's Chainring. Part I: Static and Low-Velocity Impact Analysis, submitted in *CMCA*, 2018.

Wang, Y., Ji, D., and Zhan, K., Modified Sprocket Tooth Profile of Roller Chain Drives, *Mech. Theor.*, vol. **70**, pp. 380–393, 2013.